*J. Fluid Mech.* (1985), *vol.* 150, *pp.* 203–231
*Printed in Great Britain*



# The self-induced motion of vortex sheets

By J. J. L. HIGDON AND C. POZRIKIDIS
Department of Chemical Engineering, University of Illinois, Urbana, IL 61801

(Received 11 November 1983 and in revised form 27 July 1984)

A method is presented for following the self-induced motion of vortex sheets. In this method, we use a piecewise analytic representation of the sheet consisting of circular arcs with trigonometric polynomials for the circulation. The procedure is used to study the evolution of the motion in two special cases: a circular vortex sheet with sinusoidal circulation distribution and an infinite plane vortex sheet subject to periodic disturbances. The first problem was studied by Baker (1980) as a test of the method of Fink & Soh (1978), while the second has been studied by a number of authors, notably Meiron, Baker & Orszag (1982). In each case, we follow the motion of the sheet up to the appearance of a singularity at a finite time. The singularity takes the form of an exponential spiral with the simultaneous development of singularities in the curvature and in the circulation distribution. In the final stages of the calculations, up to 155 marker points are used to specify the position of the sheet. If it were possible to execute a stable calculation with equally spaced point vortices, approximately $10^6$ points would be required to achieve the same resolution. Problems with instabilities have been reduced, but not entirely eliminated, and prevent a rigorous verification of the results obtained.

## 1. Introduction

In many areas of fluid dynamics, the flow field is characterized by sharp changes in velocity occurring in concentrated shear layers. In the asymptotic limit as the thickness of these layers approaches zero, they may be viewed as vortex sheets. The problem of following the developing motion thus becomes one of following the evolution of the vortex sheet. Unfortunately, the calculation of the self-induced motion of vortex sheets has proved to be quite intractable and has resisted the best efforts of numerous investigators.

The first attempts to calculate the deformation of a vortex sheet were those of Rosenhead (1931) and Westwater (1935), who replaced the continuous two-dimensional vortex sheet with a collection of discrete point vortices. Unfortunately, this simple straightforward procedure leads to chaotic motion which does not accurately represent the behaviour of the continuous vortex sheet. Following these initial attempts, there have been numerous efforts to modify and stabilize the point-vortex method. Noteworthy is the work of van de Vooren (1980), who showed that the principal-value integrals could be evaluated accurately through regularization of the integrand. Unfortunately, this did not appear to be the sole cause of difficulty, as his calculations led to chaotic behaviour. A comprehensive survey of vortex methods is given in the review article by Saffman & Baker (1979).

Fink & Soh (1974) analysed the errors associated with the representation as a set of discrete vortices. Their major conclusion was that the errors could be reduced significantly if the points were equally spaced along the sheet. Using a repositioning

technique after every time step, Fink & Soh demonstrated smooth roll-up calculations for a finite vortex sheet. Although the method of Fink & Soh demonstrated good results for this case, it required the use of an amalgamation model to deal with the singular behaviour at the tips of the sheet. Baker (1980) proposed a test of the method on a closed vortex sheet, for which the amalgamation procedure would be unnecessary. Baker corrected some minor errors in the analysis of Fink & Soh and applied the method to the roll-up of a circular vortex sheet with sinusoidal vorticity distribution. He found that the method was unreliable, leading to the sheet crossing itself with the problem becoming increasingly severe as the number of points was increased. Baker concluded that the smooth results obtained by Fink & Soh were primarily attributable to the strong flow induced by the amalgamated vortex, and that the method was not suitable for treating a general class of flows.

Moore (1981) has provided the most detailed analysis of the point-vortex method. He identified the difficulties as a discrete form of the well-known Helmholtz instability and showed that the most unstable mode has a period equal to twice the spacing of the vortices. As with the continuous Helmholtz instability, the fastest growth rates are for the smallest wavelengths. Thus, increasing the number of vortices merely serves to increase the growth rate of the disturbance. Moore discussed the effects of the smoothing techniques proposed by Fink & Soh and also considered a technique employed by Longuet-Higgins & Cokelet (1976). He found that both techniques improved the results, but still led to the unphysical behaviour associated with sheets crossing themselves.

With the failure of the point-vortex method in its various manifestations, a number of authors have tried alternative approaches. Moore (1979) studied periodic disturbances on an infinite plane vortex sheet by expanding the position of the sheet in a Fourier series. By analysing the decay of the coefficients at large wavenumbers, he inferred the existence of a singularity at a finite critical time. Moore's analysis was valid only for asymptotically small initial disturbances. Meiron, Baker & Orszag (1982) adopted a more general spectral method which allowed for initial disturbances of finite amplitude. Using computer-extended expansions and series enhancements, such as Padé approximants, they were able to identify singularities in the sheet curvature and in the second derivative of the circulation distribution. The critical time for the appearance of these singularities was consistent with Moore's asymptotic prediction. Meiron *et al.* presented profiles of the sheet at the critical time which showed only slight distortion on a macroscopic scale. Unfortunately, the authors did not describe the shape of the sheet near the point of infinite curvature. This could be of the form of a simple inflected curve or a spiral of imperceptible size.

One additional study has been conducted employing series enhancement techniques. Schwartz (1981) considered the roll-up of a finite vortex sheet and found that a singularity appeared in the form of an exponential spiral at the tips. This problem differs significantly from those discussed above, because the circulation is singular at the tips starting from the initial instant.

At this point, it may be helpful to summarize the state of the art in vortex motion. Vortex-sheet calculations may be divided into two broad classes: discrete methods, including the point-vortex method and its variants; and spectral methods, such as that employed by Meiron *et al.* The discrete methods may be easily applied to any set of initial conditions, but have proven unreliable, resulting in chaotic motion after a finite time. The spectral methods seem to give more reliable results, but can be implemented efficiently only for special prototype problems. These methods provide valuable tools for studying the mathematical character of the problem, but are too specialized to find general application in modelling vortex flows.

The challenge for fluid dynamicists is to find a technique that combines the flexibility of the discrete methods with the reliability of the spectral methods. In the present effort, we propose a method which makes substantial progress toward this goal. We use a higher-order discretization scheme replacing the continuous vortex sheet with a collection of circular arcs and the circulation distribution with piecewise trigonometric polynomials. The principal advantage of the method is that it does not depend on any special vortex spacing for its accuracy. Thus additional marker points may be added at any point in the calculation to resolve the fine details of the motion as they evolve. We apply this procedure to two problems which have been treated by other methods: a circular vortex sheet with sinusoidal circulation distribution (Baker 1980), and an infinite plane vortex sheet with periodic disturbances (Meiron *et al.* 1982). In each case the calculations proceed up to the appearance of a singularity at a finite time. This is in contrast with all other discrete methods, which lead to chaotic motion. The results of our calculations are broadly consistent with those of Meiron *et al.*, but show some differences in the shape of the vortex sheet.

The method we describe is not entirely stable. Instabilities may develop in the form of disturbances on the sheet whose wavelength is a function of local point spacing. Since the growth rate is most rapid for close point spacing, these instabilities limit the number of marker points and prevent a rigorous verification of our results.

## 2. Velocity induced by the vortex sheet

We consider a vortex sheet lying along a closed curve $C$ with circulation per unit length $\gamma(s,t)$, where $s$ is the arclength measured along the sheet. In standard complex notation, we may write the induced velocity as

$$q^* = u - \mathrm{i}v = \frac{1}{2\pi\mathrm{i}} \int_C \frac{\gamma(s',t)\,\mathrm{d}s'}{z - z(s',t)} \tag{1}$$

(see e.g. Batchelor 1967).

To find the induced velocity for a material point on the sheet, we take the Cauchy principal value

$$\frac{\partial z^*}{\partial t}(s,t) = \frac{1}{2\pi\mathrm{i}} \text{⨍}_C \frac{\gamma(s',t)\,\mathrm{d}s'}{z(s,t) - z(s',t)}. \tag{2}$$

To follow the evolution of the sheet, we may in principle integrate with respect to time to find the trajectory of material points on the sheet. In order to perform the integration, we require information concerning the change in $\gamma(s,t)$ as a function of time. Kelvin's circulation theorem requires that the circulation around any closed contour is conserved. Considering a contour around any differential segment of the sheet, we find that $\gamma\,\mathrm{d}s$ is a conserved quantity. In following the motion of the vortex sheet, it is convenient to choose a Lagrangian variable to identify points on the sheet. As a conserved quantity, the circulation $\Gamma$ may be chosen as the Lagrangian variable, and (2) may be written

$$\frac{\partial z^*}{\partial t}(\Gamma,t) = \frac{1}{2\pi\mathrm{i}} \text{⨍}_C \frac{\mathrm{d}\Gamma'}{z(\Gamma,t) - z(\Gamma',t)}, \tag{3}$$

as suggested by Birkhoff (1962).

We now have a nonlinear integrodifferential equation for the motion of the vortex sheet. In practice, the analytical solution of (2) and (3) is intractable, and we rely on numerical methods. The standard procedure is to identify the position of the sheet using a finite number of marker points. We then expect that the motion of the sheet

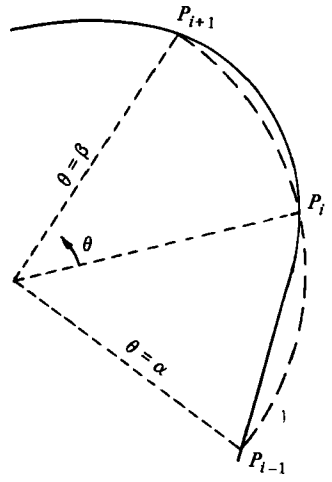


FIGURE 1. Local representation of the vortex sheet with circular arcs.

may be approximated by calculating the trajectories of the marker points. To calculate these trajectories, the integral must be approximated given only the information at the finite number of marker points. The method of approximation is what distinguishes the various approaches.

The crudest approach is the point-vortex method, replacing the continuous sheet with point distributions of circulation. The next level is the method of Fink & Soh (1978), who replace the sheet with straight segments along which the circulation has a constant value. In the present effort, we consider a higher-order approximation, using arcs along the sheet with a piecewise polynomial for the circulation. This representation has been employed previously by Mangler & Smith (1959), who used a single arc to model the inner portion of the vortex sheet shed from a delta wing. In the present circumstances, this discretization proves efficient, because the resulting integrals may all be evaluated analytically.

Proceeding with this method, let us identify the sheet by $2N$ points $P_n$. At the initial time, the position and circulation of each of these points is specified. Consider the evaluation of the velocity at the point $P_n$. Referring to figure 1, we identify a circular arc $A_n$ which passes through the three points $P_{n-1}, P_n, P_{n+1}$. We make no restrictions on the relative spacing among the points; hence $P_n$ is not necessarily at the centre of the arc. Taking a local polar coordinate system with the origin at the centre of the arc and the $x$-axis going through $P_n$, we approximate the circulation with the piecewise representation

$$\gamma = \gamma_A + \gamma_B \sin\theta, \tag{4}$$

where the coefficients $\gamma_A$, $\gamma_B$ are chosen such that the circulation between each pair of points is preserved:

$$\int_{Pn-1}^{Pn} (\gamma_A + \gamma_B \sin\theta)\, R\, \mathrm{d}\theta = \Gamma_n - \Gamma_{n-1}, \tag{5}$$

$$\int_{Pn}^{Pn+1} (\gamma_A + \gamma_B \sin\theta)\, R\, \mathrm{d}\theta = \Gamma_{n+1} - \Gamma_n. \tag{6}$$

Fitting arcs in like manner over the entire sheet, we obtain an approximation of the integral in (2) of the form

$$q_n^* = \frac{1}{2\pi \mathrm{i}} \sum_j \int_{A_j} \frac{\gamma_j(\theta)\, \mathrm{d}s}{z_n - z_j(s,t)}, \tag{7}$$

where the summation extends over all arcs on the sheet and $q_n$ is the velocity evaluated at position $z_n$.

Let us consider the error involved in this discretization. Referring to a small section of the sheet going through three adjacent points as in figure 1, let the subtended angles be $\alpha$ and $\beta$. In the local polar coordinate system, we may specify the exact location of the sheet by

$$r = R(1+f(\theta)). \tag{8}$$

Note that representing the sheet with a circular arc is equivalent to setting $f \equiv 0$.

Employing the requirement that the sheet passes through the three points, we have

$$f(\theta) = \theta(\theta-\alpha)(\theta-\beta)g(\theta), \tag{9}$$

where $g(\theta)$ is a non-singular function of $\theta$.

With the definitions above, we may write the approximate integral in the form

$$q^*_{\text{approx}} = \frac{1}{2\pi \mathrm{i}} \int_\alpha^\beta \frac{(\gamma_A + \gamma_B \sin\theta) R \,\mathrm{d}\theta}{R - R\,\mathrm{e}^{\mathrm{i}\theta}}, \tag{10}$$

and the exact integral as

$$q^*_{\text{exact}} = \frac{1}{2\pi \mathrm{i}} \int_\alpha^\beta \frac{\gamma(\theta) R[(1+f)^2 + (f')^2]^{\frac{1}{2}} \,\mathrm{d}\theta}{R - R(1+f)\,\mathrm{e}^{\mathrm{i}\theta}}. \tag{11}$$

To find the error in the representation (9), we expand each integral for small $\theta$ and evaluate at $P_i$. We assume that the circulation may be expanded in a series of the form

$$\gamma = \gamma_0 + \gamma_1 \theta + \gamma_2 \theta^2 + \ldots. \tag{12}$$

The first two coefficients in the expansion are determined to $O(\alpha^2)$ by the value of the total circulation at the three points, using conditions similar to (5).

With these expansions, the integrals may be evaluated to give

$$q^*_{\text{exact}} = q^*_{\text{approx}}(1 + O(\theta_{\text{M}}^2)), \tag{13}$$

where $\theta_{\text{M}} = \max(\alpha, \beta)$.

This analysis applies for arbitrary choice of the angles $\alpha$ and $\beta$. If we choose points equally spaced in arclength $\alpha = -\beta$, the order $\theta_{\text{M}}^2$ term is identically zero, and the error is $O(\theta_{\text{M}}^3)$, equivalent to the error obtained by Baker (1980). The strength of our method is that the error remains small $O(\theta_{\text{M}}^2)$ even when the points are not equally spaced. Thus we may add more points to resolve the fine details of the motion and use fewer points where the scale of the motion is larger. This flexibility is essential to the success of our calculations.

When the vortex sheet is of infinite length with periodic disturbances, we cannot implement the outlined procedure directly, because of the infinite interval of integration. Instead, we use the expression for a periodic line of vortex singularities. Thus, in place of (2), we have

$$\frac{\partial z^*}{\partial t}(s,t) = \frac{1}{2\lambda \mathrm{i}} \text{⨍}\!\!\!\!\!\!-\!\!\!\!\!\!\int_{C_\lambda} \cot\left[\frac{\pi}{\lambda}(z(s,t) - z(s',t))\right] \gamma(s',t)\,\mathrm{d}s', \tag{14}$$

where $C_\lambda$ represents the part of $C$ in a single wavelength.

To evaluate this integral for a point $z_0$, we adopt the following approach. First, we define $I_1$ to be the integral (2) over a single wavelength centred on $z_0$. We subtract $I_1$ from (14), yielding an integral $I_2$ whose integrand is non-singular:

$$I_2 = \frac{1}{2\lambda \mathrm{i}} \text{⨍}\!\!\!\!\!\!-\!\!\!\!\!\!\int_{C_\lambda} \left\{\cot\left[\frac{\pi}{\lambda}(z(s,t) - z(s',t))\right] - \frac{\lambda}{\pi} \frac{1}{z(s,t) - z(s',t)}\right\} \gamma(s',t)\,\mathrm{d}s'. \tag{15}$$

This integral may be evaluated using standard quadrature formulas. In practice, a simple trapezoid rule is usually sufficient, because the limiting source of error is in the evaluation of $I_1$, which is calculated using the method described earlier.

## 3. Numerical procedure

The analysis of §2 provides an efficient method for evaluating the induced velocity at all points on the vortex sheet. To implement this method in calculating the deformation of the sheet, we proceed as follows. The position of the sheet is specified by choosing $N$ points equally spaced along the sheet, and the circulation at these points is determined from the initial conditions. This sets up the calculations for the first time step.

At the beginning of each time step, the arcs are laid out between the marker points. If the angle subtended by any arc exceeds a pre-established maximum, additional marker points are added according to the interpolation scheme described below. When the arcs have been properly assigned, the piecewise circulation distributions are calculated. The integrals are then evaluated to obtain the velocity at each marker point. The new positions of the marker points are calculated using the modified Euler method with an error of order $(\Delta t)^2$. As the calculation proceeds, the time step is continually adjusted, such that the maximum angle subtended by the arcs does not exceed a specified limit during the time step. In practice, the need to add additional marker points at frequent intervals is the major restriction on the length of the time step. Thus the use of a higher-order integration algorithm is unwarranted.

We now consider the method used to insert additional marker points. Assume that the arc $A_n$ that passes through the points $P_{n-1}$, $P_n$, $P_{n+1}$ is larger than the prescribed limit. We construct a temporary arc $A'$ through points $P_{n-1}$, $P_n$ with curvature equal to the mean curvature of arcs $A_{n-1}$ and $A_n$. Similarly, we construct arc $A''$ through $P_n$, $P_{n+1}$ with curvature equal to the mean of arcs $A_n$ and $A_{n+1}$. Consider now the composite curve made up of $A'$ and $A''$. We divide this curve into three segments of equal length and place a new marker point at the ends of each segment. To maintain an even point distribution, we eliminate the original point $P_n$. The circulation at the new marker points is calculated from the previous circulations using four-point Lagrangian interpolation with respect to arclength.

The rather involved procedure for inserting new points is based on a very simple principle. It is designed such that the curvature as a function of arc length varies smoothly over the entire sheet. Simpler methods that produce kinks in the curvature distribution rapidly lead to instabilities at the location of newly inserted points.

## 4. The roll-up of a circular vortex sheet

In this section we present some results for the self-induced motion of a circular vortex sheet with a sinusoidal distribution of circulation $\gamma = \gamma_0 \cos\theta$. This vortex sheet represents that shed by a thin circular rim or ring wing at small angles of incidence. More importantly, it provides an attractive test case for studying the dynamics of vortex sheets without the additional complication of end points. Experiments (Bofah 1975) indicate that the sheet should roll up into a pair of spirals. Calculations using the method of Fink & Soh were attempted by Baker (1980), but broke down owing to instabilities.

Our calculations started with 40 points evenly spaced around the circle. As the motion developed, additional points were inserted with the criterion that the

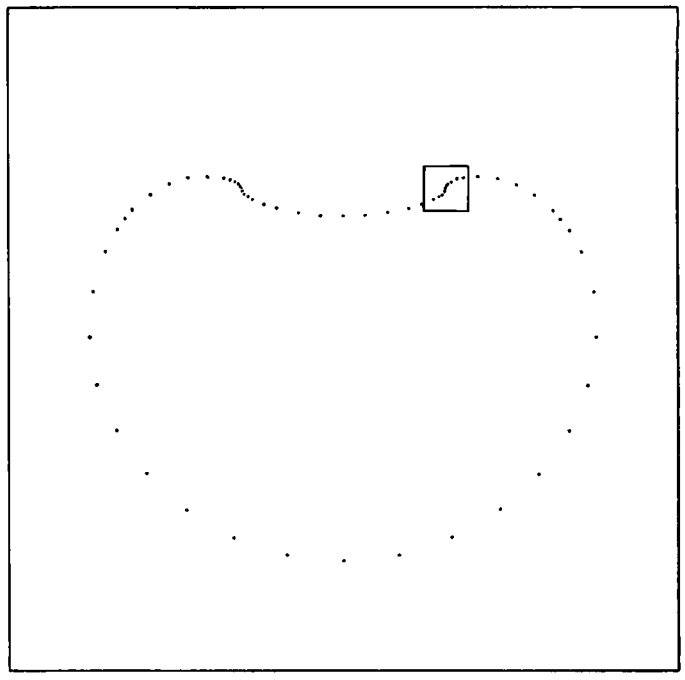

FIGURE 2. Profile of an initially circular sheet at $t' = 1.30$. Rectangle indicates area of close-up shown in later figures.

maximum angle subtended by an arc be less than 0.55. In the final stages of the motion the maximum angle was allowed to increase to 0.75. At the final step there were 155 points along the sheet. The calculations were repeated with an initial distribution of 32 points with a maximum angle of 0.75. The profiles obtained were quite similar, but did show some variation from the previous results; the time required for the roll-up differed by approximately 5%. More quantitative comparisons will be left to the end of this section. Attempts to repeat the calculations with smaller subtended angles were sensitive to the onset of instabilities, especially in the later stages. Improvements in the point-insertion technique or the addition of a smoothing technique might help to alleviate these problems. The large number of marker points required by smaller subtended angles led to rapidly increasing computation costs, which tended to discourage further experimentation. The computations for the results presented in this section required approximately 4 minutes of CPU time on a CDC CYBER 175.

The time step used with the modifed Euler method was changed continually from an initial time step $\Delta t' = 0.02$ to a time step $\Delta t' = 0.000003$ in the final stages of the calculation. The time $t'$ is non-dimensionalized with respect to $\gamma_0$ and the radius $a$, i.e. $t' = \gamma_0 t/a$.

The shape of the sheet at time $t' = 1.30$ is shown in figure 2. We see that the sheet has begun to roll up as expected, with the largest change over the top half of the sheet. This figure may be interpreted as the end of the first phase of the roll-up process.

During the short interval of time following $t' = 1.30$, we see the rapid emergence of a spiral over a small portion of the sheet. Close-up views of the central portion of the spiral at successive times and increasing magnification are shown in figure 3. The area covered by each close-up is shown by the small rectangle in the preceding figure. Owing to the rapidly decreasing timescale as the spiral develops, only the central portion of the spiral undergoes significant change over the time considered.

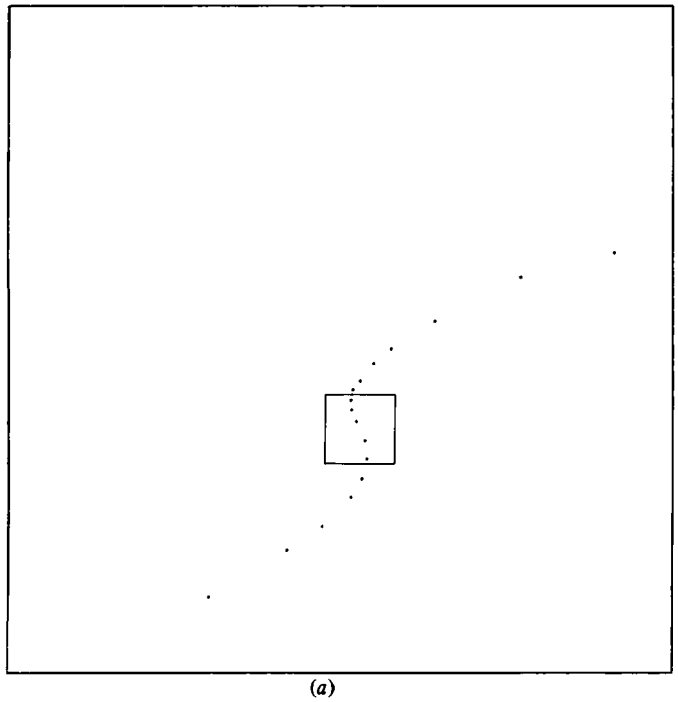

(a)

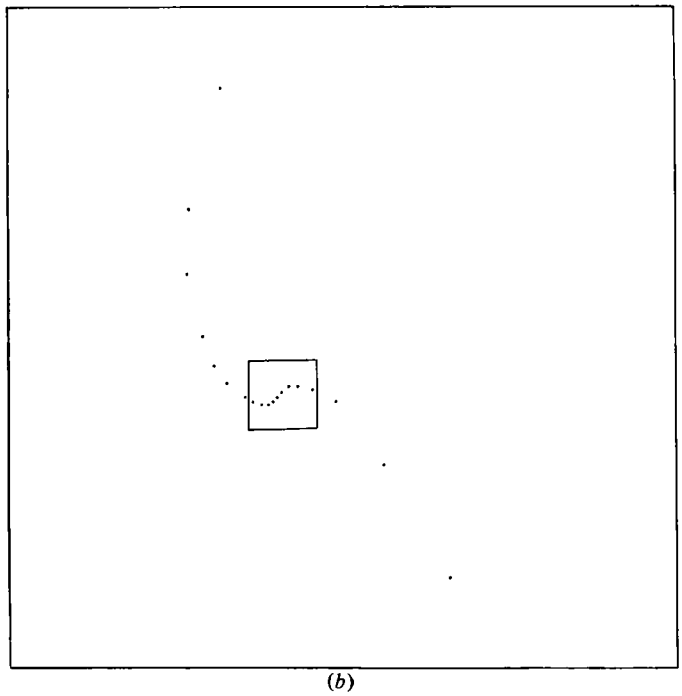

(b)

FIGURE 3(a, b). For caption see facing page.

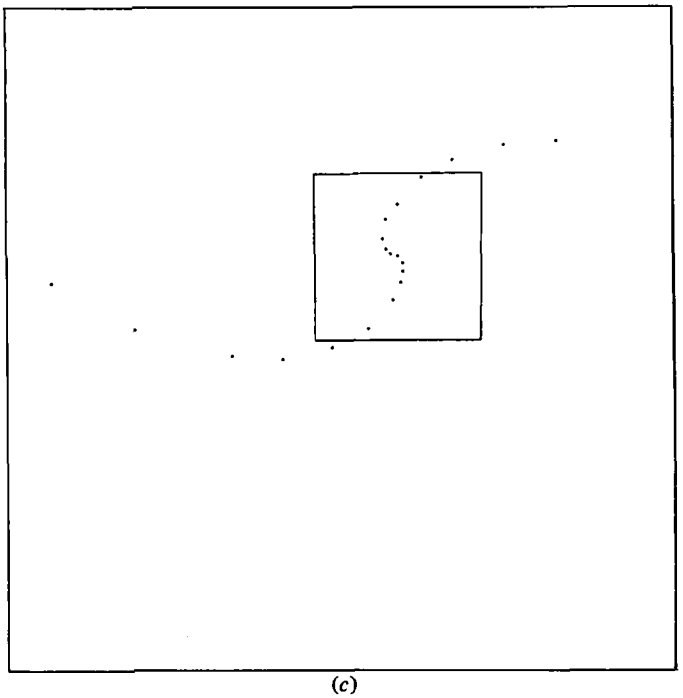

(*c*)

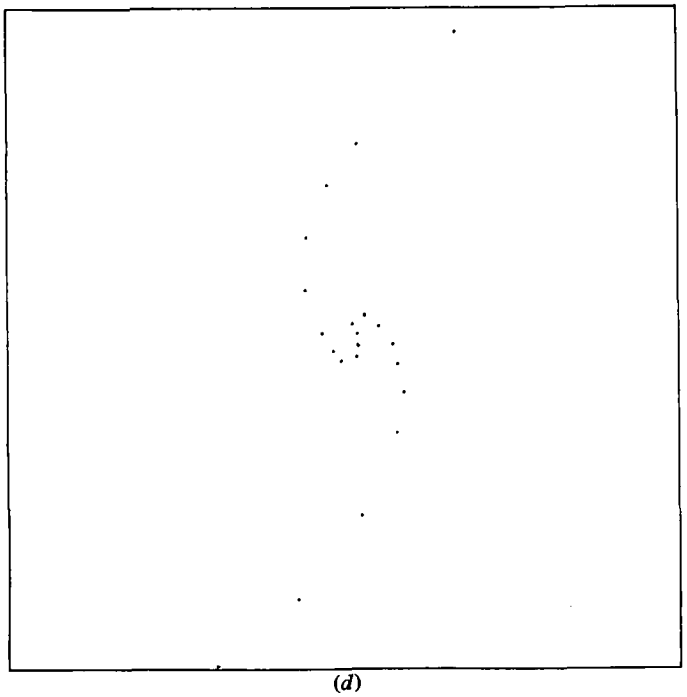

(*d*)

FIGURE 3. Magnified views of the central portion of the spiral at successive times. Rectangle shows area covered by following close-up. (*a*) 15 ×, $t' = 1.31226$; (*b*) 150 ×, 1.31456; (*c*) 1500 ×, 1.3145936; (*d*) 6000 ×, 1.3145966.

Thus the portion of each spiral outside the rectangle is effectively unchanged at later instants. In particular, we note that the shape of the sheet at the time $t' = 1.31$ would appear identical with the shape as shown in figure 2, if we were unable to see the extremely small details revealed in the close-up views.

As we examine the successive views shown in figure 3, we see a strong similarity in the shapes of the curves, even as the lengthscale changes by three orders of magnitude. This similarity is characteristic of an exponential spiral of the form $r = A\,\mathrm{e}^{-b\theta}$. To determine if these profiles do in fact correspond to an exponential spiral, we plot $\ln r$ versus $\theta$ in figure 4. We see that there is excellent agreement between the calculated points and the double-branched spiral which appears as the pair of lines in figure 4(*a*). The points near the bottom of each line which veer sharply away represent the central portion of the spiral which has not fully developed at this instant of time. Figure 4(*b*) shows the correspondence of the exponential spiral with the calculated profiles.

Figures 3 and 4 show that an extremely fine structure develops on the sheet over a very short space of time. To resolve the details of this structure up to the time considered, it is clear that the spacing between marker points must be of the order of that shown in figure 3(*d*). If it were possible to repeat these calculations with a point-vortex method, the number of equally spaced points required would be of the order of $10^6$. Thus it is not surprising that the method of Fink & Soh as applied by Baker (1980) with a maximum of 91 points failed to resolve the details of the exponential spiral.

Up to this point we have shown that the emerging spiral shows a strong resemblance to an exponential spiral, but we have not shown that a singularity, i.e. a fully developed spiral with an infinite number of turns and infinite curvature, develops in a finite time. To do this, we require a measure of the rate at which the spiral is emerging. The most convenient method is to consider the minimum radius of the arcs going through the calculated points. The radius of curvature of the spiral is of order $r \sim \mathrm{e}^{-b\theta}$; hence it is equal to zero only when $\theta \to \infty$. Thus an infinite number of turns will have developed when the radius of curvature goes to zero and the curvature becomes infinite. Figure 5 shows the minimum radius of the arcs plotted versus time. This clearly shows that the radius of curvature approaches zero at a critical time approximately equal to 1.31459+. Thus we see that a singularity appears in the shape of the sheet at a finite time and have tentatively identified the singularity as an exponential spiral $r \sim \mathrm{e}^{-1.4\theta}$.

At this time, we retrace our steps and consider the behaviour of the circulation distribution as the sheet develops its spiral. Figure 6 shows the circulation $\gamma$ over the central portion of the spiral, plotted versus arclength. The portion of the sheet shown corresponds approximately to the portion of the spiral shown in figure 3(*a*). The four instants of time correspond to those of figures 3(*a–d*) respectively. We note that the area under the curve in each figure remains constant, as required by the conservation of circulation. As the motion proceeds towards the critical time, the circulation develops a strong peak in the centre of the spiral. This indicates that the small centre segment undergoes compression, while the adjacent arms are being stretched.

In figure 6 we noted that the peak circulation increased rapidly with time. To determine if it develops a singularity at a finite time, we plot the inverse of the maximum circulation versus time in figure 7. It is clear that this quantity approaches zero, i.e. that the circulation becomes singular at a finite critical time. The value of $t_{\mathrm{cr}}$ from this curve appears identical with that obtained for the curvature singularity.

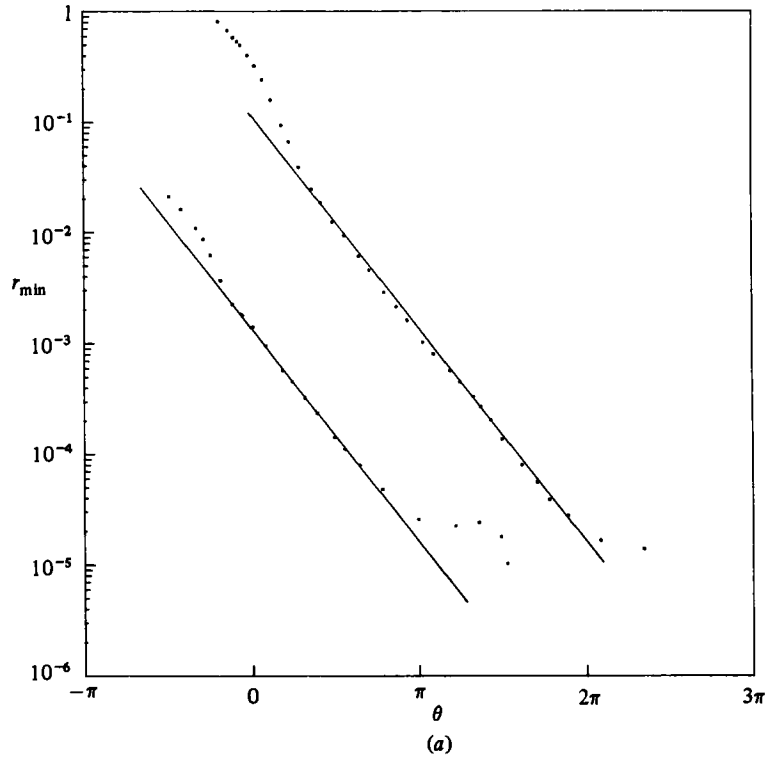


(*a*)

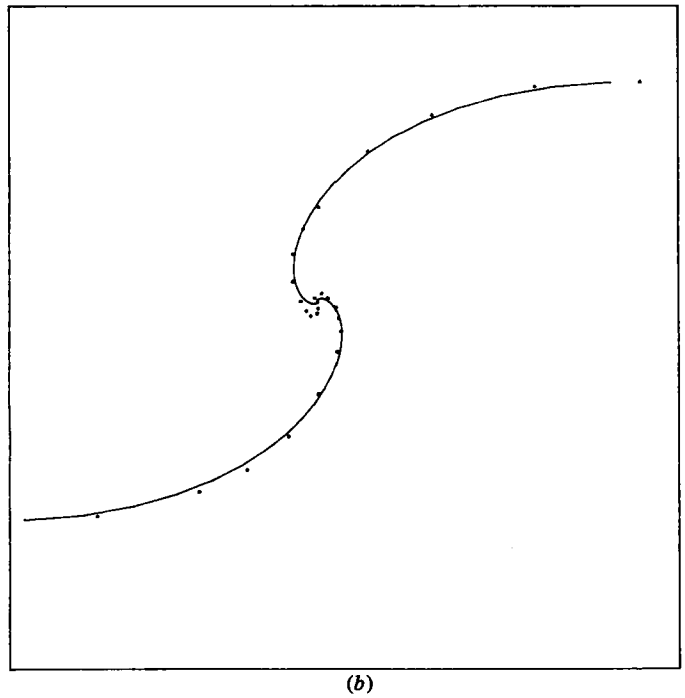

(*b*)

FIGURE 4. (*a*) Plot of ln $r$ versus $\theta$ showing comparison with exponential spiral. Straight line represents a double-branched spiral, $\ln r = -1.413\theta - 2.16$, $\ln r = -1.413(\theta+\pi) - 2.16$.

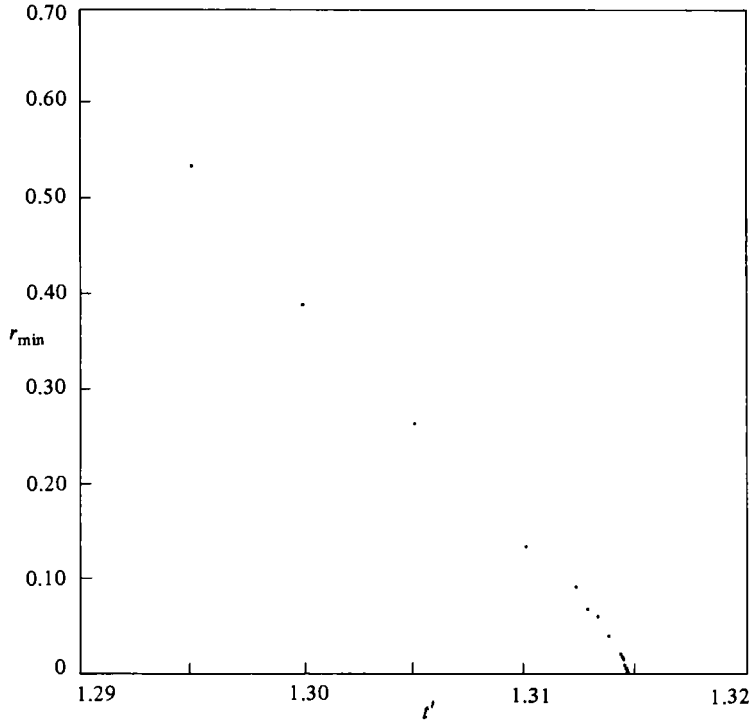


FIGURE 5. Minimum radius of curvature versus time.

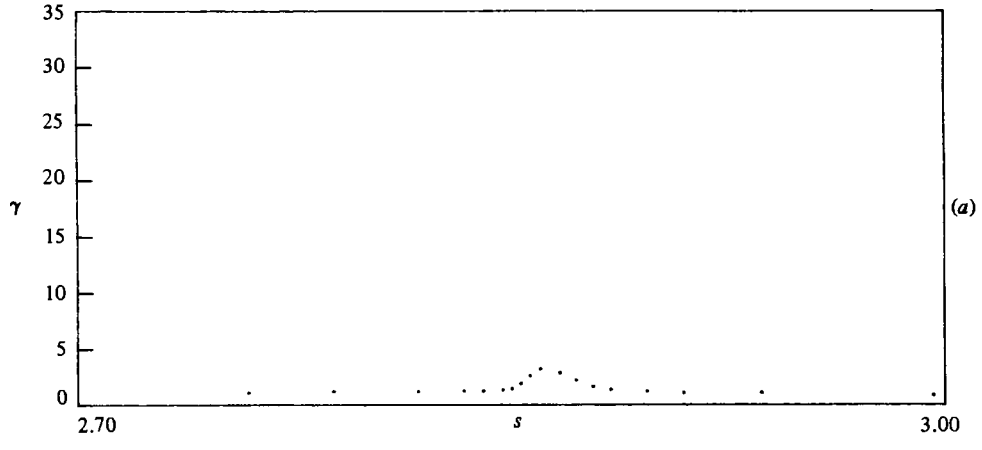


FIGURE 6(a). For caption see facing page.

The simultaneous appearance of singularities in the curvature and in the circulation is not surprising. Both are a consequence of the rapidly diminishing lengthscale and timescale in the centre of the spiral. Proceeding with this idea, we suppose that the roll-up in the spiral is governed by the local flow with a single characteristic length and time. These characteristic values may be determined from the maximum curvature $\kappa$ and maximum circulation $\gamma$. Dimensional reasoning then dictates the form of the equations relating $\kappa$ and $\gamma$. The analysis in the Appendix shows that $\kappa$

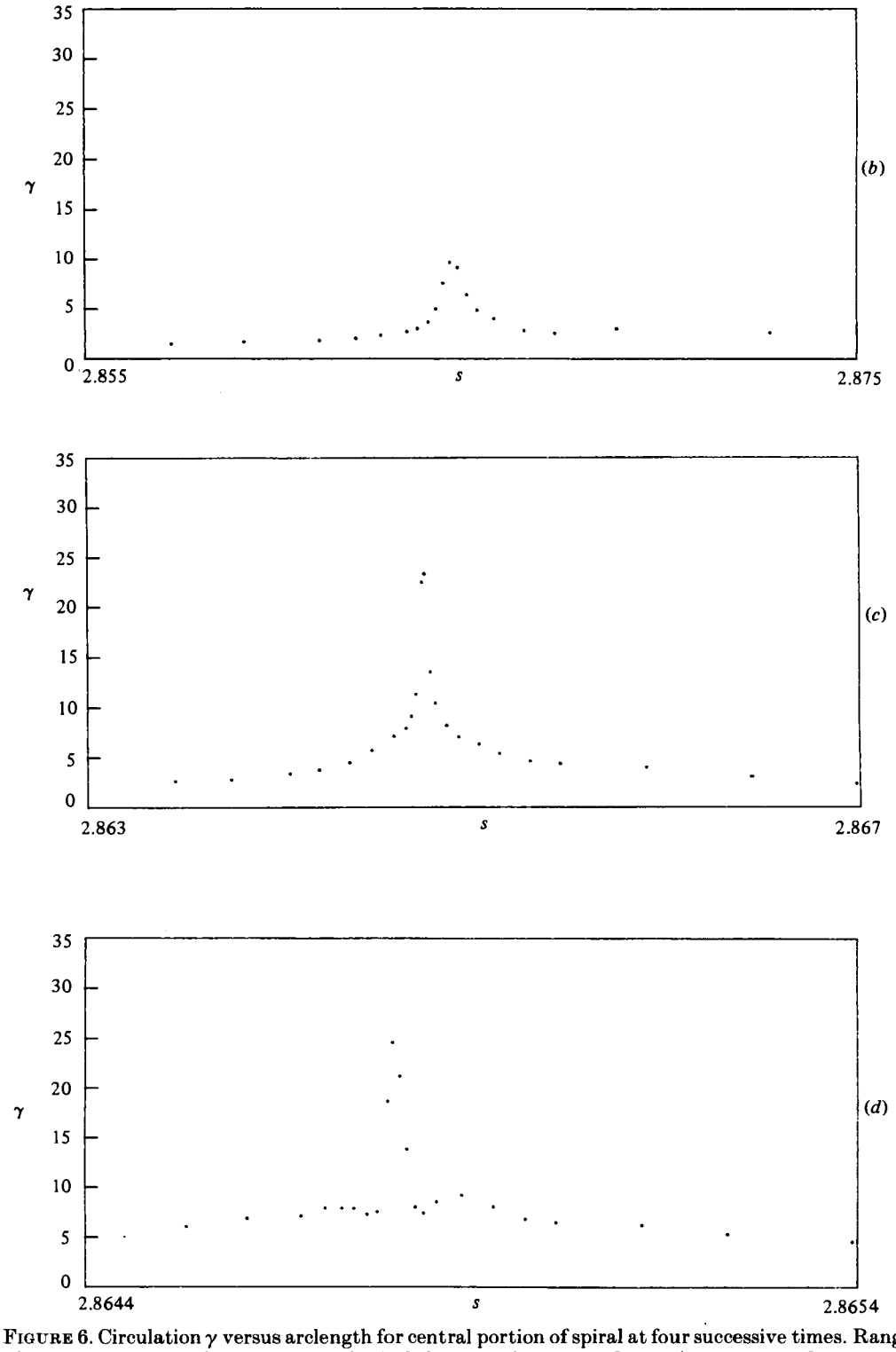


FIGURE 6. Circulation $\gamma$ versus arclength for central portion of spiral at four successive times. Range of abscissa corresponds to portions of spiral shown in figure 3(*a–d*). (*a*) $t' = 1.31226$; (*b*) 1.31456; (*c*) 1.3145936; (*d*) 1.3145966.

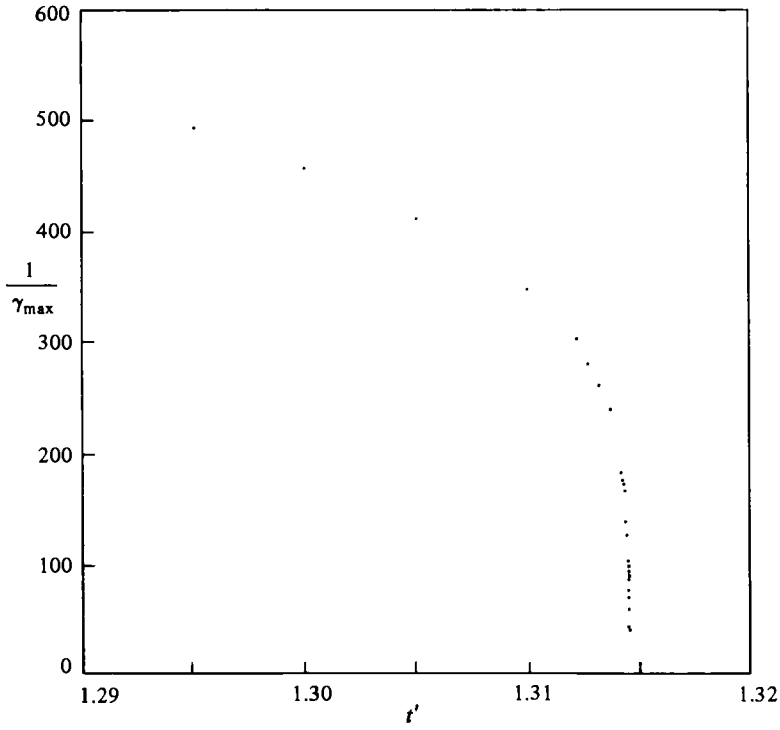


FIGURE 7. Inverse of maximum circulation versus time.

and $\gamma$ should possess algebraic singularities with the sum of the exponents equal to $-1$.

To obtain values for these exponents from our numerical results, we plot $\kappa$ and $\gamma$ versus $t_{cr}-t$ on logarithmic scales in figures 8 (*a*, *b*). The lines on these figures represent least-squares fits. From the slopes of the lines we have

$$\kappa \sim (t_{cr}-t)^{-0.751}, \quad \gamma \sim (t_{cr}-t)^{-0.257}$$

The sum of the exponents is $-1.008$, which compares well with the required value of $-1$. We emphasize that the exponents for $\kappa$ and $\gamma$ were determined independently.

We make one further test to assess the validity of this similarity analysis. The second derivative of $\gamma$ with respect to arclength provides a second lengthscale in the spiral region. If the state of the motion truly depends on a single lengthscale then $\gamma''$ should scale as $\kappa^2\gamma$. Usng the exponents from above, this indicates that

$$\gamma'' \sim (t_{cr}-t)^{-1.759}.$$

A plot of $\gamma''$ versus $t_{cr}-t$ is shown in figure 8 (*c*). The line on this figure represents the exponent just given, and is not a recursion line drawn through the points. This figure shows that the values of $\gamma''$ are quite consistent with the proposed similarity solution.

The local analysis we have presented completes the description of the roll-up process. The only task remaining is to verify the reliability of the numerical results. One test is to evaluate the momentum and kinetic energy associated with the flow. These are conserved quantities and should remain invariant throughout the motion. Both quantities may be evaluated as integrals along the sheet (see e.g. Batchelor 1967, §7.2). The $x$-component of momentum is zero by symmetry. The $y$-momentum has a maximum relative error of $10^{-4}$. The kinetic energy has a relative error of $5 \times 10^{-4}$.

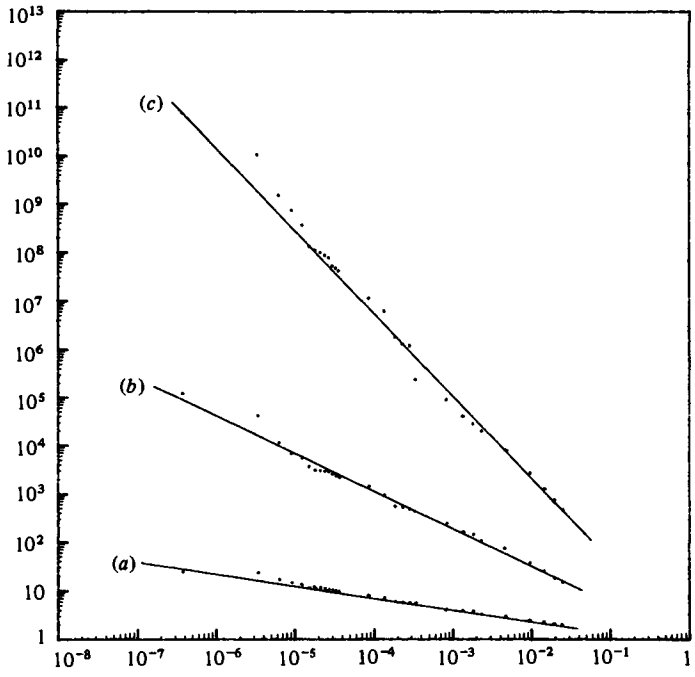


FIGURE 8. Singular quantities versus $t_{cr}-t$ on logarithmic scales; slope indicates exponent of singularity: (*a*) circulation $\gamma$; (*b*) curvature $\kappa$, (*c*) $\gamma'' = \mathrm{d}^2\gamma/\mathrm{d}s^2$.

As another test of the numerical results, the calculations were repeated with an initial distribution of 32 points. The critical time increased by 5% to 1.38. The location of the spiral shifted downward by $0.04a$, where $a$ is the initial radius of the circle. This vertical shift is consistent with the later critical time, because the entire sheet moves downward as it rolls up. The spiral shifted horizontally a distance $0.002a$. The most significant change was in the shape of the sheet near the centre of the spiral. The 40 point calculation gave $r \sim \mathrm{e}^{-1.4\theta}$, while the 32 point calculation gave $r \sim \mathrm{e}^{-1.7\theta}$. We conclude that our calculations provide a good description of the roll-up, but cannot give an exact result for the shape of the sheet at the critical time.

## 5. Periodic disturbances on a plane vortex sheet

In this section we present the results of calculations for an initially flat vortex sheet with uniform circulation, subject to a periodic disturbance in the circulation. This corresponds to the problem studied by Meiron *et al.* (1982). The initial circulation is specified in the form

$$\gamma = 1 + a\cos x,$$

where $x$ is dimensionless and $\gamma$ has been non-dimensionalized with respect to the uniform circulation $\gamma_0$; $a$ is the amplitude of the disturbance.

For the calculations presented here, the sheet was represented by 20 points initially, increasing to 70 points in the final stages of the calculation. The maximum subtended arc was 0.40 for the early stages of the calculation and 0.80 for the final stages. We were unable to use a larger number of points owing to the onset of instabilities. The calculations were repeated with an initial distribution of 14 points and a maximum angle of 1.14. The latter results were consistent with the more refined calculations and will be described in more detail at the end of this section.

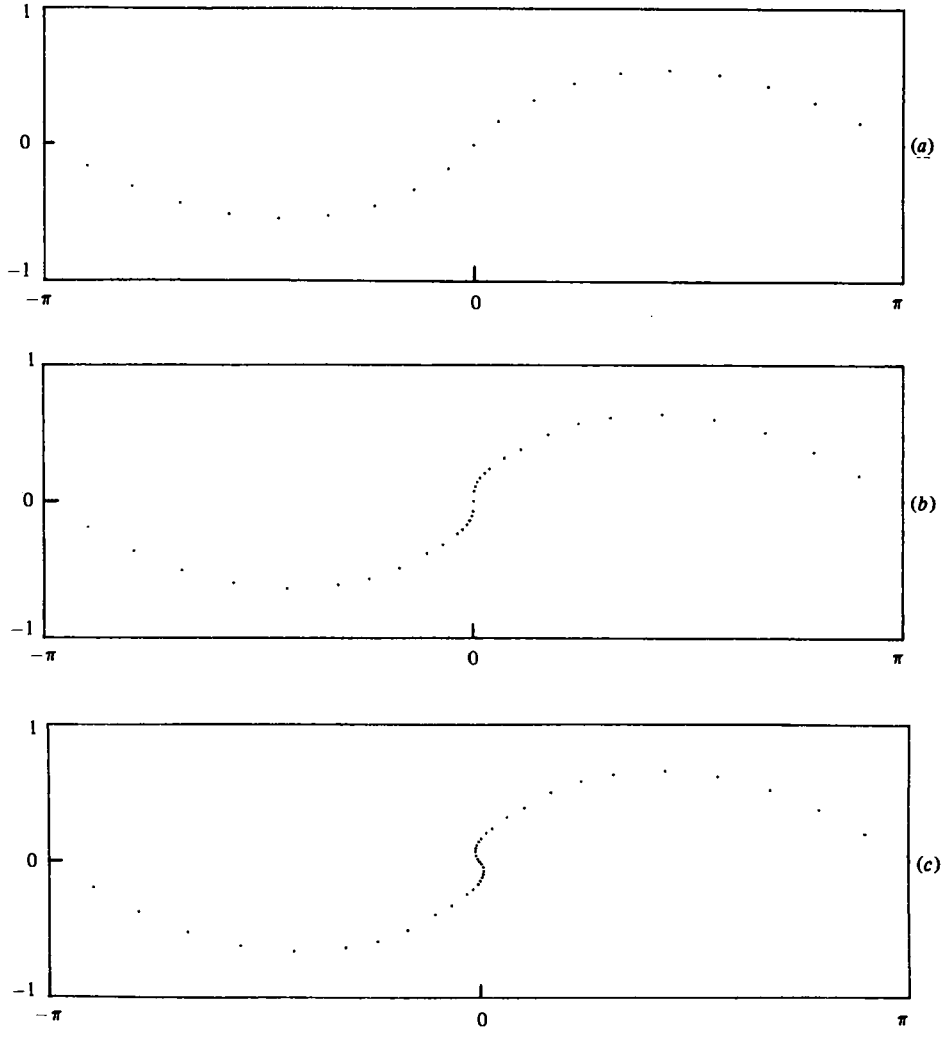


FIGURE 9(*a*, *b*, *c*). For caption see facing page.

The profiles of the vortex sheet at six successive instants of time are shown in figures 9(*a–f*). The initial disturbance in the circulation had amplitude $a = 1$. In figure 9(*a*) we see the shape of the sheet at the end of the initial stage of the evolution. The sheet differs only slightly from a sinusoidal profile which would be predicted by a linearized theory. A short time later (figure 9*b*) there is a marked change in the shape of the sheet at the centre of the wavelength. At this instant the centre of the sheet has become vertical, indicating the final instant at which the shape could be represented as a single-valued function of $x$. In figure 9(*c*) the sheet has continued past the vertical and has started to roll up around the centre point. At succeeding instants, the roll-up process continues (figure 9*d–f*) over the small central region, with barely perceptible changes over the remainder of the sheet.

To appreciate the emergence of the extremely fine details at the centre of the spiral, we must examine close-up views of this section. Figures 10(*a–c*) show a 50× magnification for the three profiles shown in figures 9(*d–f*). We see that approximately one quarter turn of the spiral develops between each pair of figures; however, the

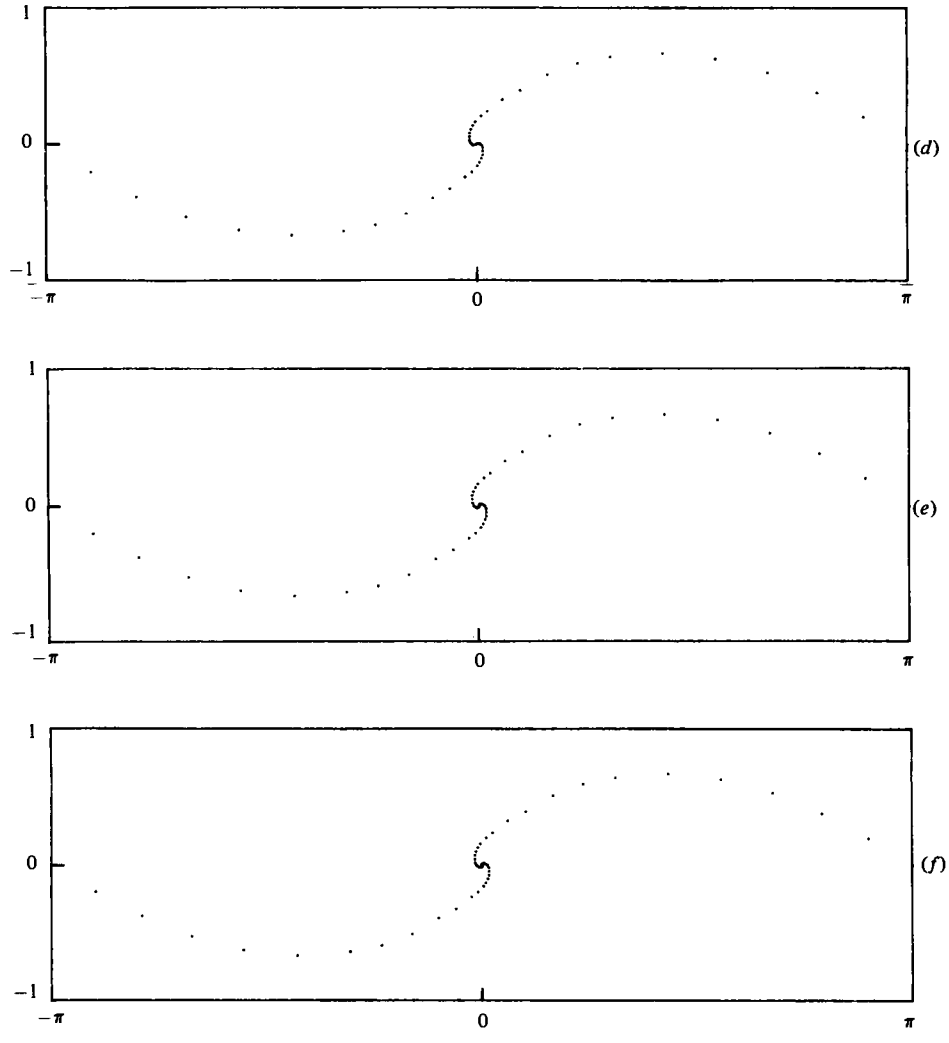


FIGURE 9. Profile of the periodic vortex sheet at successive instants. (*a*) $t = 1.01$; (*b*) 1.301; (*c*) 1.341; (*d*) 1.359; (*e*) 1.3636; (*f*) 1.36385.

time required for this development decreases drastically from $\Delta t = 0.0046$ to $\Delta t = 0.00025$. Thus the roll-up process accelerates as it progresses.

The shape of the innermost region of the spiral remains remarkably similar as it rotates and decreases in size. This similarity is characteristic of an exponential spiral of the form $r \sim e^{-b\theta}$. To make a more quantitative comparison, we plot $\ln r$ versus $\theta$ in figure 11(*a*). The continuous line drawn through the points gives a value of $b = 0.953$. The two points veering sharply away from the line at the bottom of the figure represent the points at centre, where the roll-up is incomplete. Figure 11(*b*) shows a comparison of the exponential spiral with the calculated profile from figure 10(*c*).

The sequence of profiles in figures 9 and 10 indicate that the vortex sheet rolls up in the form of an exponential spiral; however, at the times shown only the first turns of the spiral have emerged. A fully developed spiral has an infinite number of turns with a singularity in the curvature at its centre. It is clear that the present spiral

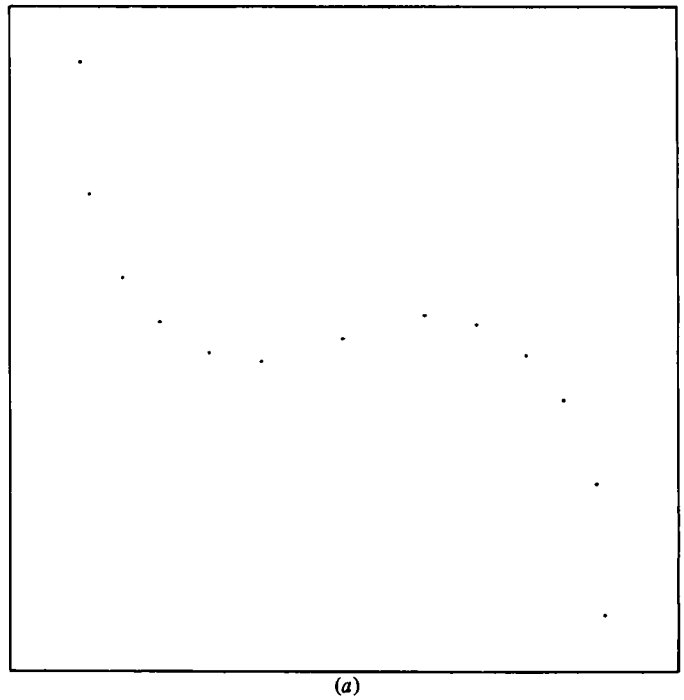

(a)

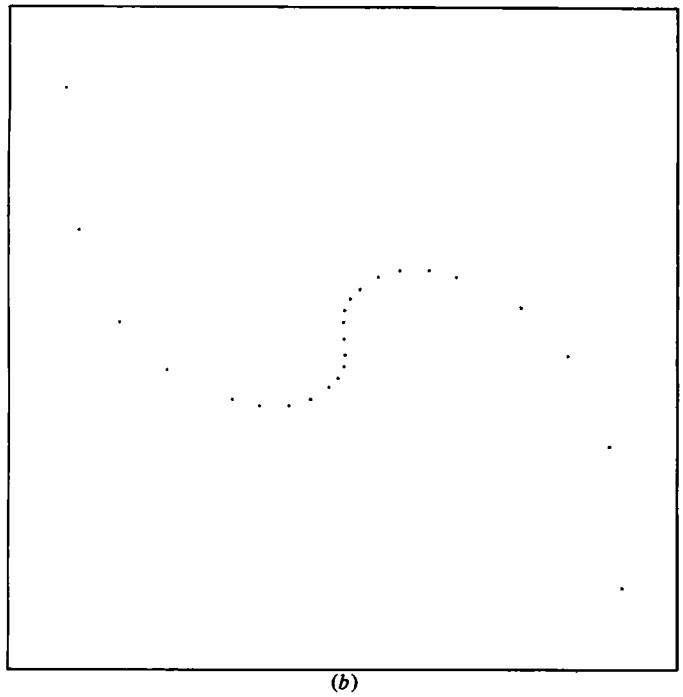

(b)

FIGURE 10(a, b). For caption see facing page.

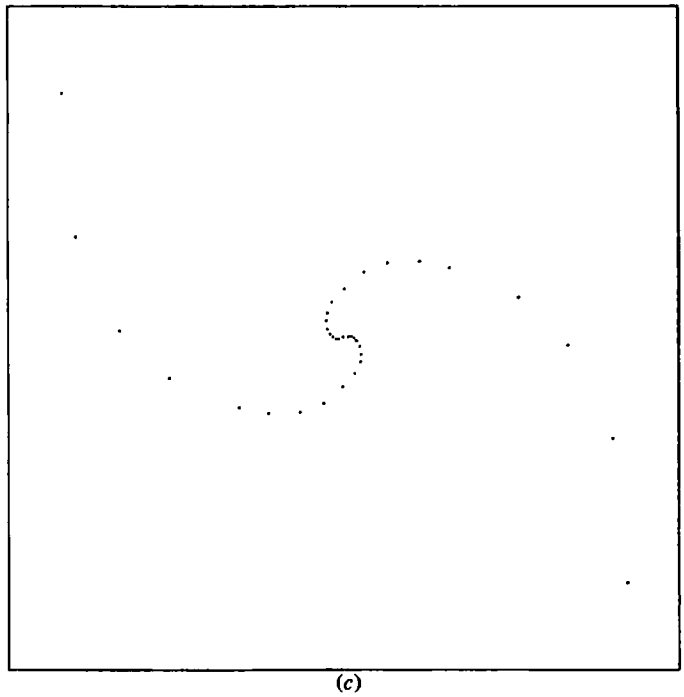

(*c*)

FIGURE 10. Magnified view (50 ×) of the central portion of the spiral during the roll-up process. Profiles correspond to last three instants in figure 9.

will continue to roll up at an ever increasing rate; the only question is whether the complete roll-up will occur in a finite time. To address this point, we plot the minimum radius of curvature occurring on the sheet as a function of time. Figure 12 shows a clear trend indicating zero radius, and hence infinite curvature, at a time slightly before $t = 1.364$. Thus we infer the existence of a singularity in curvature at a finite critical time. The behaviour of the curvature in the neighbourhood of the critical time will be discussed further at the end of this section.

At this point we turn our attention to the distribution of circulation along the sheet. Figures 13 (*a–f*) show the circulation as a function of arclength at successive instants of time. These six figures correspond to the profiles shown in figures 9 (*a–f*). The general trend is toward a concentration of circulation in the centre of the spiral, with an ever-sharpening peak. Recalling that the circulation is equal to the jump in velocity across the vortex sheet, we see that the fluid is continually accelerating, while the lengthscale decreases rapidly. This combination of increasing velocity and decreasing lengthscale explains the diminishing timescale, and hence the appearance of a singularity at a finite time. Earlier we noted the singularity in sheet curvature; now we see evidence for the possibility of a singularity in the curvature distribution. As before, we test this by plotting the inverse of the maximum circulation versus time (figure 14). While not quite as clearly as in the previous case, this figure does show that $1/\gamma$ approaches zero at a finite time, i.e. that the circulation becomes infinite.

To investigate the behaviour of the curvature and the circulation in the neighbourhood of the critical time, we consider a local analysis as discussed in §4. As before, we anticipate algebraic singularities and plot $\kappa$ and $\gamma$ versus $t_{cr}-t$ on logarithmic axes (figures 15*a*, *b*). The solid lines in this figure give the values for the exponents

$$\kappa \sim (t_{cr}-t)^{-0.869}, \quad \gamma \sim (t_{cr}-t)^{-0.288}.$$

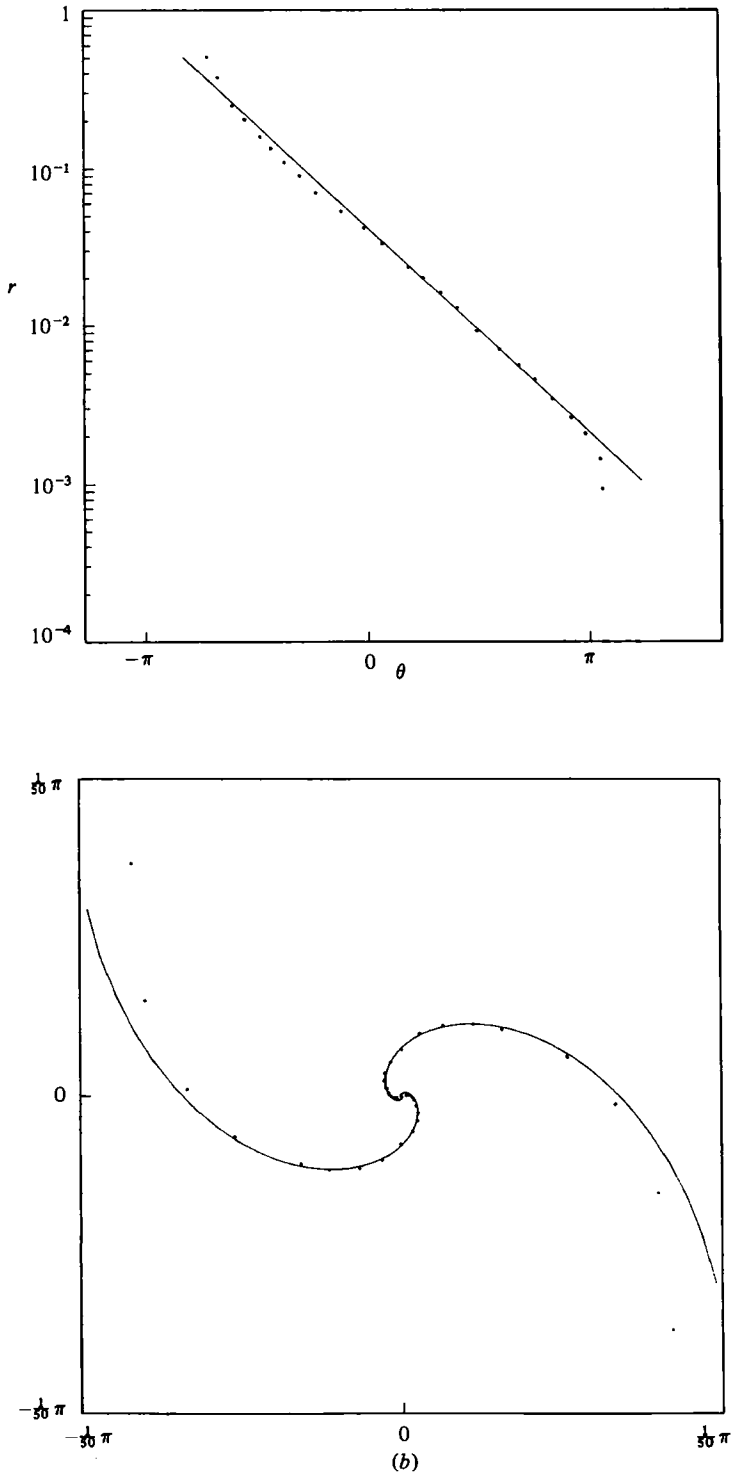


FIGURE 11. (*a*) Plot of $\ln r$ versus $\theta$ for the spiral. Solid line represents exponential spiral $\ln r = -0.953\theta - 3.148$. (*b*) Comparison of the exponential spiral with the actual profile of sheet.

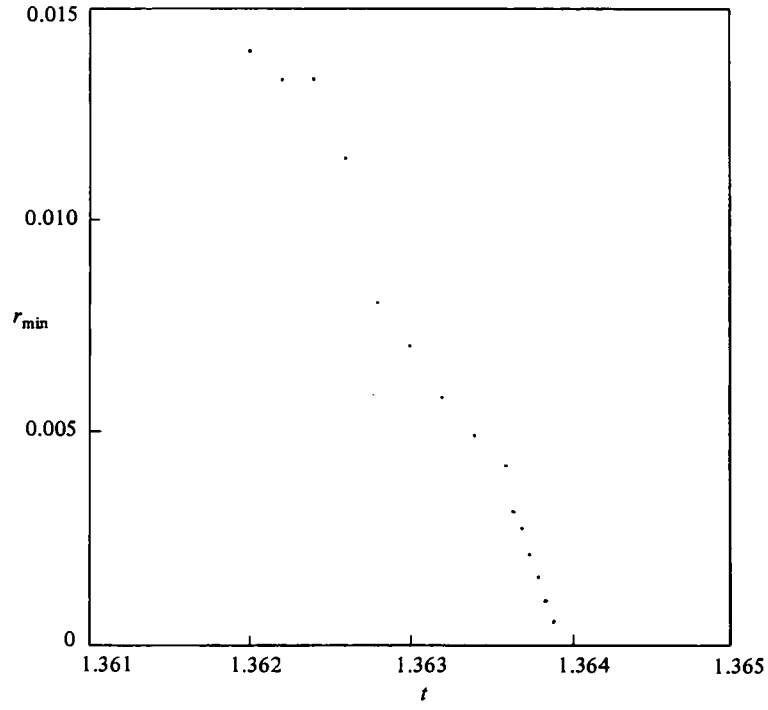


FIGURE 12. Minimum radius of curvature versus time.

As a consistency check, we note that the sum of the exponents should be $-1$. The actual value of $-1.157$ is reasonable considering the simplicity of the scaling analysis and the inexactness of the numerical results.

As a further test, we note that $\gamma''$ should scale as $\kappa^2\gamma$. Figure 15(*c*) shows fair agreement with this scaling, where the points are numerically calculated values of $\gamma''$ and the solid line corresponds to $\kappa^2\gamma$. It should be pointed out that the points at the top of this figure are very sensitive to the value of $t_{cr}$. A shift of 0.0001 in the value of $t_{cr}$ would bring these points into line while affecting the other points very little.

As with the circular sheet, the accuracy of the calculations for periodic disturbances is limited by instabilities, which prevent a finer resolution of the motion. To check the invariants, we calculated the kinetic energy and found a relative error of $10^{-4}$. The momentum in this case is identically zero from symmetry. A crude consistency check was performed by repeating the calculations with an initial distribution of 14 points and a maximum subtended angle of 1.14. In this calculation the behaviour was essentially the same, with the critical time increasing by 16%, and the shape of the sheet changing by 2% with the coefficients $b$ increasing from 0.953 to 0.970.

## 6. Discussion

The two problems in vortex motion that we have considered were chosen in part because they had previously been attacked using other methods. We wish to compare the results of our calculations with those previous results. For the circular sheet, our calculations demonstrate the appearance of a singularity at a finite time, while previous calculations using the method of Fink & Soh (Baker 1980) broke down owing

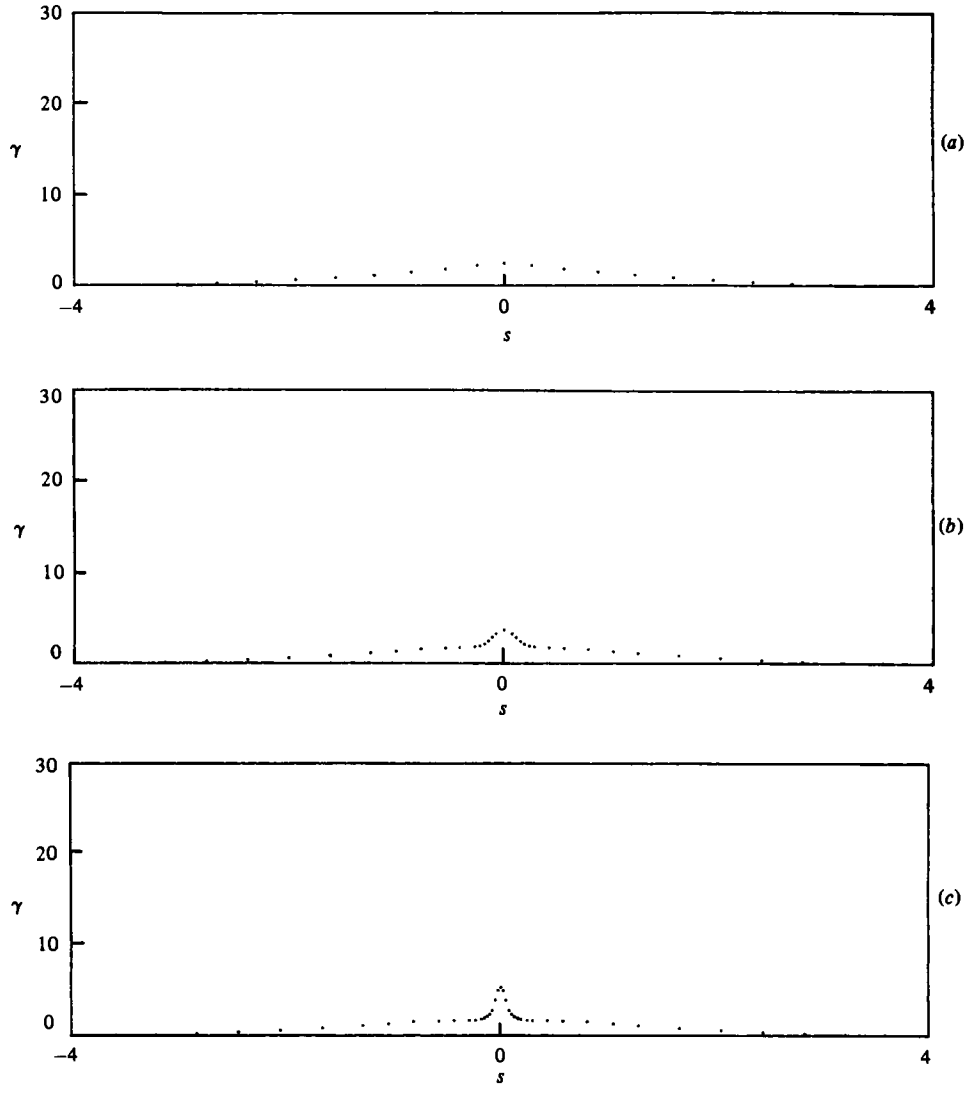


FIGURE 13(*a*, *b*, *c*). For caption see facing page.

to instabilities. This is not surprising, because the use of equally spaced points prevents a resolution fine enough to resolve the singularity.

For the periodic disturbances, we compare with the calculations of Meiron *et al.* (1982, hereinafter referred to as MBO). First, we consider the predictions for the critical time. Figure 16 shows a plot of $t_{cr}$ versus initial amplitude. The solid line is the asymptotic prediction of Moore (1979). The results of the three methods are broadly consistent with our calculations, overestimating the critical time by approximately 25%. This is not surprising, as we saw a 16% variation arising from different point spacings. A partial explanation for this variation lies in the fact that all discrete methods underestimate the growth rate for the shortest waves. In our method the growth rate for these waves is underestimated by 44% compared with 50% for the point-vortex method. This error is offset somewhat by the fact that the shortest wavelength in our calculations is continually decreasing as additional points

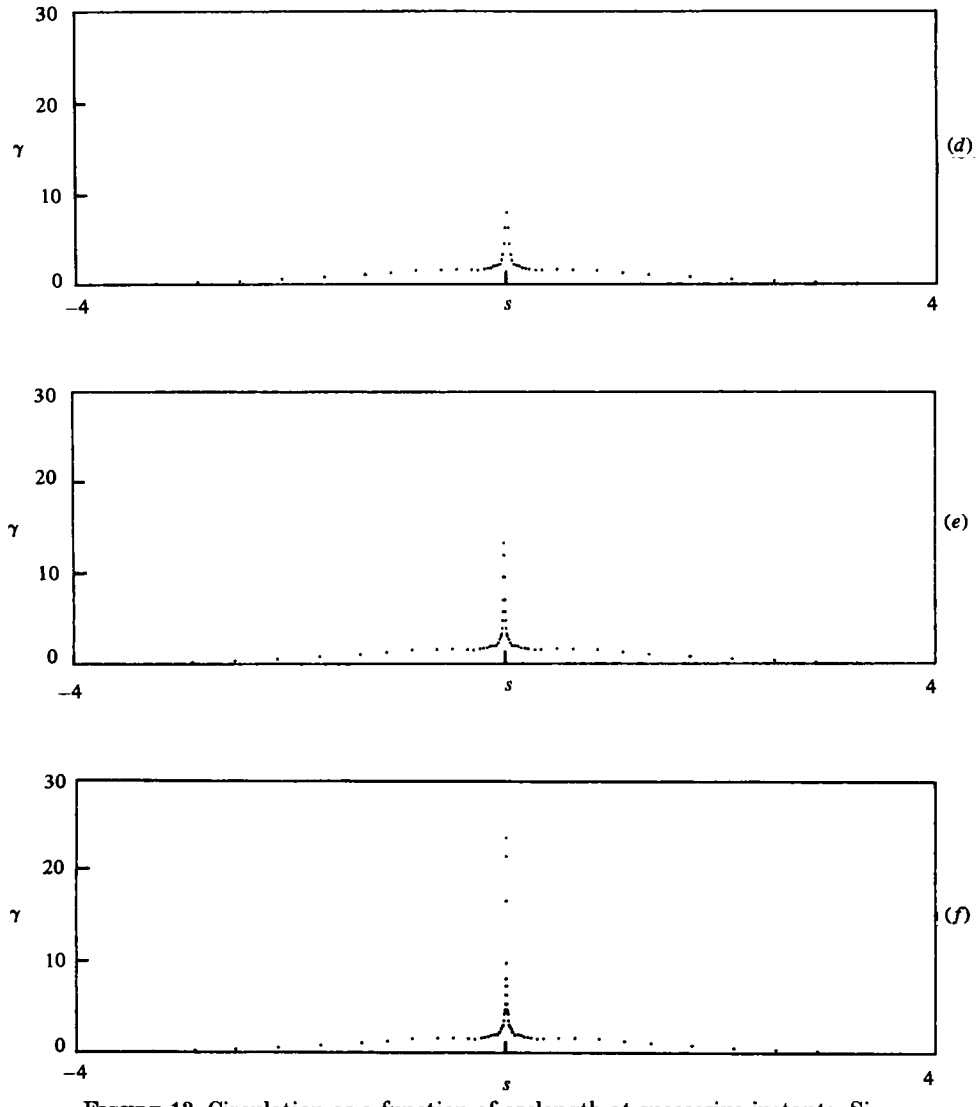


FIGURE 13. Circulation as a function of arclength at successive instants. Six instants (*a*)–(*f*) correspond to figures 9(*a*–*f*) respectively.

are added. Nonetheless, we conclude that our results probably overestimate the critical time. MBO based their estimates on a series analysis, which should give more reliable values for $t_{cr}$.

The most important comparison concerns the form of the singularities predicted by the calculations. Here we find agreement on two points – both groups predict singularities in the sheet curvature and in the second derivative of circulation $\gamma''$; however, there is disagreement on the circulation $\gamma$ (referred to as $\omega$ in MBO's notation). Our calculations show a singularity in $\gamma$; MBO show a peak in $\omega$, but of finite value. In addition, the profiles of the vortex sheet presented by MBO do not exhibit the roll-up discovered here. The discrepancies we have noted lie in the local description of the sheet. Before attempting an explanation for these differences, we consider a comparison of global quantities.

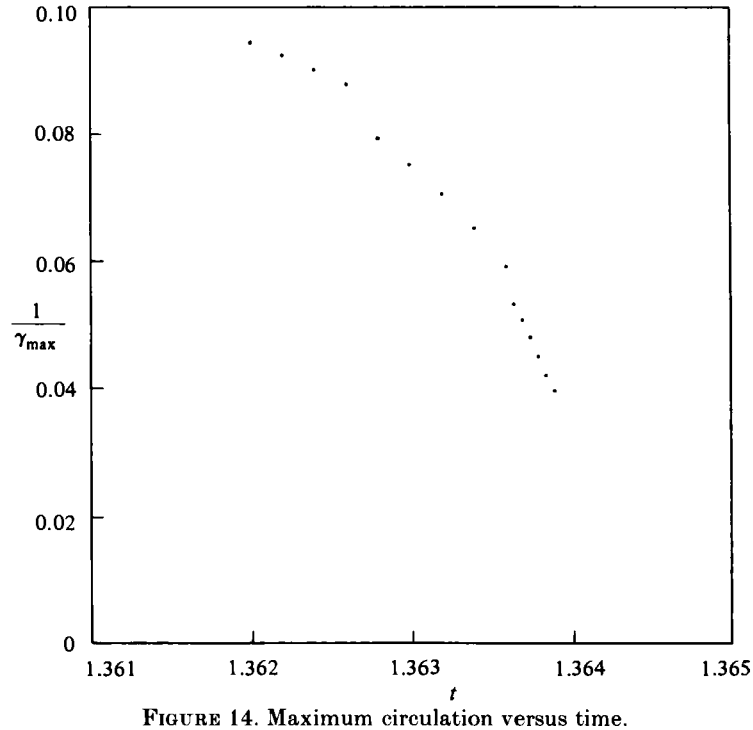


FIGURE 14. Maximum circulation versus time.

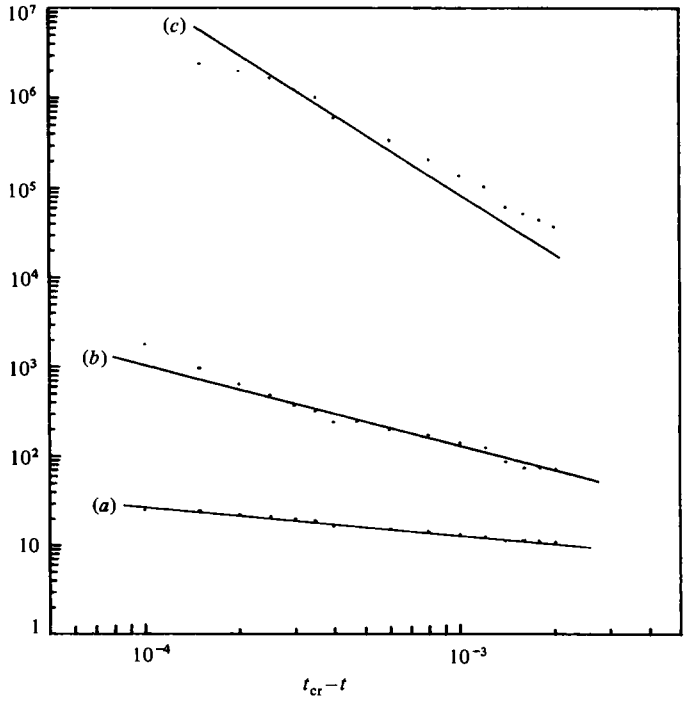


FIGURE 15. Singular quantities versus $t_{cr}-t$ on logarithmic scales: (*a*) circulation $\gamma$; (*b*) curvature $\kappa$; (*c*) $\gamma'' = d^2\gamma/ds^2$.

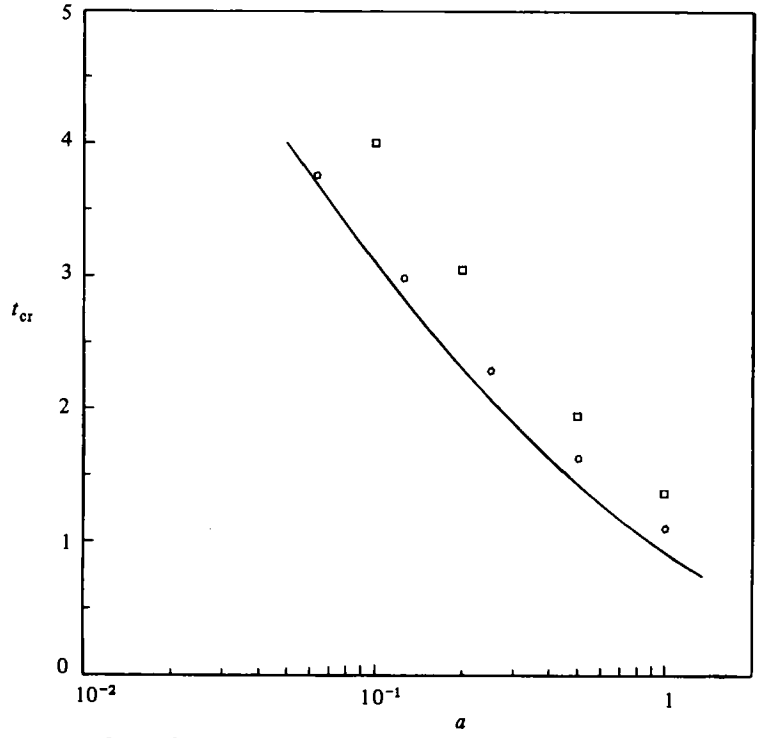


FIGURE 16. Critical time versus amplitude of disturbance: asymptotic result of Moore (1979); ○, Meiron *et al.* (1982); □, present results.

MBO inferred the existence of singularities by considering the mean-square gradients, defined as

$$\Omega^{(p)} = \int \left| \frac{\partial^p z}{\partial e^p} \right|^2 \mathrm{d}e,$$

where $e$ is a Lagrangian variable specifying position along the sheet.

By analysing the Taylor series in time, the authors identified singularities of the form

$$\Omega^{(p)} \sim (t_{\mathrm{cr}} - t)^{-\delta(p)} \quad \text{or} \quad \Omega^{(p)} \sim (t_{\mathrm{cr}} - t)^{-\delta(p)} \ln |t_{\mathrm{cr}} - t|.$$

The location of the singularity $t_{\mathrm{cr}}$ and the exponent $\delta(p)$ may be determined from a graphical representation called a Domb–Sykes plot (see e.g. Gaunt & Guttmann 1974). This plot makes use of the fact that the ratio of the Taylor coefficients approaches a limiting value in the vicinity of a singularity. In the notation of MBO,

$$R_n^{(p)} \approx \frac{1}{t_c^2}\left[1 - \frac{1-\delta}{n} + O\left(\frac{1}{n^2}\right)\right],$$

where $R_n = c_n/c_{n-1}$ and $c_n$ are the coefficients in the Taylor series. In this case the series proceeds in powers of $t^2$; $c_n$ is the coefficient of the term $O(t^{2n})$.

MBO used a linear extrapolation to estimate $\delta(2) = -0.5 \pm 0.1$. They did not give values for $\delta(3)$ or $\delta(4)$. To obtain values for all three exponents, we fitted linear regression lines for each of $\Omega^{(2)}$, $\Omega^{(3)}$ and $\Omega^{(4)}$. The values for $\delta(p)$ are given in table 1. The error estimates given represent the range of values obtained when the number of regression points was varied from the last 4 to the last 9 values of $1/n$. The error

| | MBO – linear fit | MBO – quadratic fit | Present results |
|---|---|---|---|
| $t_{cr}$ | $1.074 \pm 0.004$ | $1.079 \pm 0.001$ | $1.364 \pm 0.3$ |
| $\delta(2)$ | $0.47 \pm 0.03$ | $0.14 \pm 0.02$ | $0.06 \pm 0.05$ |
| $\delta(3)$ | $-1.22 \pm 0.05$ | $-1.69 \pm 0.03$ | $-0.95 \pm 0.05$ |
| $\delta(4)$ | $-3.34 \pm 0.01$ | $-3.45 \pm 0.05$ | $-2.10 \pm 0.20$ |

TABLE 1. Comparison of critical times and singular exponents

estimate for $t_{cr}$ represents the total range of values obtained in the individual estimates from $\Omega^{(2)}$, $\Omega^{(3)}$ and $\Omega^{(4)}$.

Although the linear estimates for $\delta(p)$ would appear to be fairly accurate, care must be taken, because it is well known that Domb–Sykes plots may be slow to converge to asymptotic slopes (van Dyke 1974). To examine the possibility, we fitted the same points to a quadratic equation and determined the slope and intercept at $1/n = 0$. The values obtained from this quadratic extrapolation are given in table 1. As can be seen, the values for $\delta(2)$ and $\delta(3)$ have changed significantly. We note that the independent estimates for $t_{cr}$ fall within a narrower range, which tends to support this extrapolation.The use of polynomial regression lines is similar to the use of a Neville table, which gives information only for the intercept. We do not wish to argue the merits of one extrapolation over another, but merely wish to point out the degree of uncertainty in the determination of the exponents $\delta(p)$.

Having obtained estimates for the singularities from the results of MBO, we turn now to our own results. In our formulation, we have calculated $z(\Gamma, t)$. These values were converted to MBO's variable $e$, and $e$-derivatives and integrals were evaluated using Lagrangian interpolation formulas. The values of $\Omega^{(p)}$ were calculated at each time step and plotted versus $1-(t/t_{cr})^2$ on logarithmic axes (figure 17). In the case of $\Omega^{(2)}$, $\mathrm{d}\Omega^{(2)}/\mathrm{d}t$ was plotted, because the function itself approaches a finite value at $t = t_{cr}$. The slopes of these lines give estimates for $\delta(p)$, which are listed in table 1. These values are qualitatively consistent with those of MBO. The difference in the numerical values is of the same order as the variation due to extrapolation technique in MBO's results. Our value for $\delta(4)$ may be off somewhat, owing to the fact that it represents the 4th derivative of numerical data. Overall, we conclude that the discrete method developed here and the spectral method of MBO give consistent results in these global measures of the singular behaviour.

Another way to compare the two calculations is in the asymptotic behaviour of the Fourier coefficients $A_n$ for large $n$. $A_n(t)$ is the Fourier coefficient for $z(e,t)$. MBO estimated the Fourier coefficients at the critical time using Padé approximants. They found that $A_n$ decayed as $n^{-\beta}$, where $\beta = 2.7 \pm 0.2$. We evaluated the Fourier coefficients numerically in the final step of our calculation and found $\beta = 2.3 \pm 0.2$. For reference, Moore's asymptotic results give $\beta = 2.5$. Thus all methods predict a divergent Fourier series for the second derivative.

We return now to the question of the local description of the sheet. The sheet profiles presented by MBO are calculated from finite Fourier series for $z(e)$. This approach is limited by the use of a small number of terms ($\sim 15$) in the Fourier series. This truncation of the infinite series constitutes a severe smoothing of the sheet. MBO demonstrated the existence of a curvature singularity, but their computed profiles show no evidence of this. Even if the curvature singularity were only a simple inflection, it would appear as a small region of large curvature, gradually becoming sharper as more Fourier modes were added. The complete absence of this behaviour

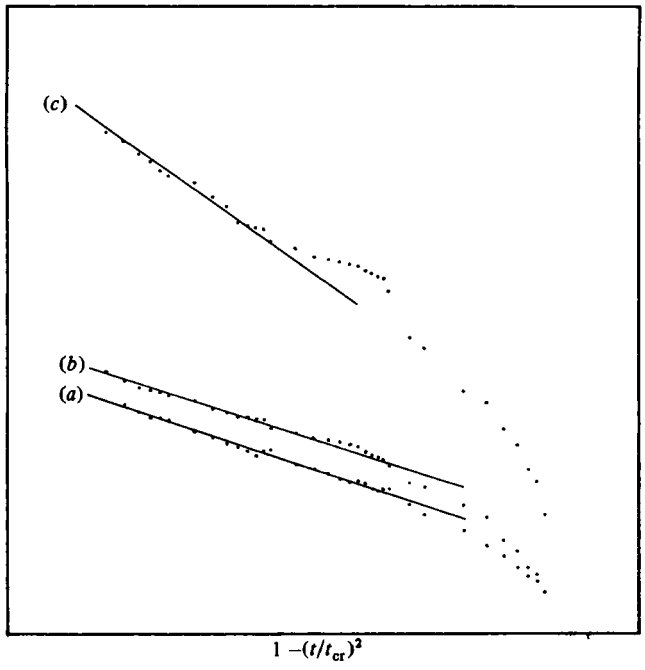


FIGURE 17. Mean-square gradients versus $1-(t/t_{cr})^2$ on logarithmic scales: (*a*) $d\Omega^{(2)}/dt$; (*b*) $\Omega^{(3)}$; (*c*) $\Omega^{(4)}$.

shows that the truncated Fourier series is insufficient to resolve the local structure in the neighbourhood of the singularity.

Finally, we consider the question of the singularity in $\gamma$. MBO employed a Lagrangian sheet strength $\gamma_e = d\Gamma/de$. This was an ideal choice for their calculations, but makes their results insensitive to a singularity in $\gamma = d\Gamma/ds$. In the MBO formulation, infinite sheet strength $\gamma$ would appear as $|dz/de| \to 0$ as $t \to t_{cr}$. This is much harder to identify from the series analysis than singularities in $z$. Moreover, this quantity approaches zero at a single point on the sheet. As with calculations of the sheet profiles, such resolution of local detail is probably beyond the limits of the truncated Fourier series.

Comparing our results with Moore's (1979) calculations, we find that Moore predicts

$$z(\Gamma, t) = \Gamma + O\left(\frac{1}{\ln(4/\epsilon)}\right) h(\Gamma)$$

near the critical time. Since his theory is valid only for small initial $\epsilon$, his calculations cannot consistently predict $dz/d\Gamma = 0$. Thus the theory does not extend to the amplitudes considered here, and there is no conflict with the present results.

In conclusion, we find that the results of our vortex calculations are largely consistent with previous results. Spectral methods as employed by MBO give more reliable estimates of the critical time, while the discrete calculation gives a better description for certain local details. In other respects, the methods give comparable results. In this paper we have shown that discrete methods may be used successfully in the analysis of vortex motion. We have provided a detailed description of the roll-up process and the resulting appearance of singularities. In its present form, the method is far from perfect, but represents a significant improvement over previous methods.

## Appendix. Local analysis of spiral region

We suppose that the circulation and curvature in the spiral region depend only on the local values. Choosing the maximum curvature and the maximum circulation as characteristic values, we require

$$\frac{1}{\gamma}\frac{\mathrm{d}\gamma}{\mathrm{d}t} = c_1 \kappa\gamma, \tag{A 1}$$

$$\frac{1}{\kappa}\frac{\mathrm{d}\kappa}{\mathrm{d}t} = c_2 \kappa\gamma \tag{A 2}$$

on dimensional grounds. $c_1$ and $c_2$ are constants associated with the motion.

These equations may be combined to give

$$\frac{\mathrm{d}}{\mathrm{d}t}\left(\frac{1}{\kappa\gamma}\right) = -(c_1+c_2). \tag{A 3}$$

It follows that $1/\kappa\gamma$ is a linear function of time, equal to zero at some time which we call $t_{\mathrm{cr}}$. Thus we may write

$$\frac{1}{\kappa\gamma} = -(c_1+c_2)(t-t_{\mathrm{cr}}). \tag{A 4}$$

Solving independently for $\kappa$ and $\gamma$, we find

$$\gamma \sim (t_{\mathrm{cr}}-t)^{-c_1/(c_1+c_2)}, \quad \kappa \sim (t_{\mathrm{cr}}-t)^{-c_2/(c_1+c_2)}. \tag{A 5}$$

## REFERENCES


Baker, G. R. 1980 A test of the method of Fink & Soh for following vortex-sheet motion. *J. Fluid Mech.* **100**, 209–220.

Batchelor, G. K. 1967 *An Introduction to Fluid Dynamics*. Cambridge University Press.

Birkhoff, G. 1962 Helmholtz and Taylor instability. *Proc. Symp. Appl. Maths Am. Math. Soc.* **13**, 55–76.

Bofah, K. K. 1975 Ph.D. thesis, California Institute of Technology.

Fink, P. T. & Soh, W. K. 1974 Calculation of vortex sheets in unsteady flow and applications in ship hydrodynamics. In *Proc. 10th Symp. Naval Hydrodynamics, Cambridge, Mass.*, pp. 463–488.

Fink, P. T. & Soh, W. K. 1978 A new approach to roll-up calculations of vortex sheets. *Proc. R. Soc. Lond.* A **362**, 195–209.

Gaunt, D. S. & Guttmann, A. J. 1974 Asymptotic analysis of coefficients. In *Phase Transitions and Critical Phenomena*, vol. 3. Academic.

Helmholtz, H. von 1868 Über discontinuirliche Flüssigkeitsbewegungen. *Monatsber. Akad. Wiss. Berlin 1868*, pp. 215–228.

Longuet-Higgins, M. S. & Cokelet, E. L. 1976 The deformation of steep surface waves on water. I. A numerical method of computation. *Proc. R. Soc. Lond.* A **350**, 1–26.

Mangler, K. W. & Smith, J. H. B. 1959 A theory of the flow past a slender delta wing with leading edge separation. *Proc. R. Soc. Lond.* A **251**, 200–217.

Meiron, D. I., Baker, G. R. & Orsag, S. A. 1982 Analytical structure of vortex-sheet dynamics. Part 1. Kelvin–Helmholtz instability. *J. Fluid Mech.* **114**, 283–298.

Moore, D. W. 1979 The spontaneous appearance of a singularity in the shape of an evolving vortex sheet. *Proc. R. Soc. Lond.* A **365**, 105–119.

Moore, D. W. 1981 On the point vortex method. *SIAM J. Sci. Stat. Comp.* **2**, 65–84.

Pozrikidis, C. 1983 M.S. thesis, University of Illinois.

PULLIN, D. I. 1982 Numerical studies of surface tension effects in nonlinear Kelvin–Helmholtz and Rayleigh–Taylor instability. *J. Fluid Mech.* **119**, 57–532.

ROSENHEAD, L. 1931 The formation of vortices from a surface of discontinuity. *Proc. R. Soc. Lond.* A **134**, 170–192.

SAFFMAN, P. G. & BAKER, G. R. 1979 Vortex interactions. *Ann. Rev. Fluid Mech.* **11**, 95–122.

SCHWARTZ, L. W. 1981 A semi-analytical approach to the self induced motion of vortex sheets. *J. Fluid Mech.* **111**, 475–490.

VAN DE VOOREN, A. I. 1980 A numerical investigation of the rolling up of vortex sheets. *Proc. R. Soc. London* A **373**, 67–91.

VAN DYKE, M. 1974 Analysis and improvement of perturbation series. *Q. J. Mech. Appl. Maths* **27**, 423–450.

WESTWATER, F. L. 1935 Rolling up of the surface of discontinuity behind an aerofoil of finite span. *Aero. Res. Comm. R. & M.* 1692.